An Embedded System Design for a Two-Axis Camera Platform Control used in Unmanned Aerial Vehicles

Franco P. L. Franco[1] and Denis S. Loubach[1] and André R. Fioravanti[1]

***Abstract*— The use of unmanned aerial vehicles (UAVs) to perform various tasks such as product delivery, aerial photography, surveillance and precision agriculture has become increasingly common. Most of the UAV applications use cameras to carry out these tasks. Generally, the cameras are stabilized by platforms known as gimbals, *i.e.* camera platform, which in turn must react to UAV attitude to minimize the disturbance in the camera. Therefore, the gimbal control becomes essential to allow capturing stable pictures and videos with almost no image processing. Considering this context, this paper introduces a low-cost (*i.e.*, $\approx$ USD 110) embedded system design and implementation for a two-axis camera platform control used in UAVs. The proposed implementation takes into account the background of three different domains: mechanical, computing and electronics. The main goal is to have a gimbal able to stabilize a camera, with respect to UAV attitude, using permanent magnetic synchronous motors as actuators. Our design also uses an inertial measurement unit (IMU) as a sensor and a proportional-integral-derivative (PID) controller. Simulated and experimental results show that the developed embedded system was able to successfully respond to a simulated UAV flight envelope, reacting in real-time and minimizing those disturbances.**

I. INTRODUCTION

The use and popularity of unmanned aerial vehicles (UAVs) have grown substantially [1]. Their functionalities are different for civilian and military purposes. Surveillance, mapping, product delivery and aerial photography are widely used today. New applications come up with innovative technology and research. Many applications require cameras that enable UAVs to perform their tasks. Therefore, they use camera platforms, also known as **gimbals**, to reduce disturbance with respect to UAV attitude. This enables the UAV to capture aerial photography and videos [1] with minimum image processing.

Therefore, the gimbal control becomes essential to allow capturing stable pictures and videos with almost no image processing. Inertial navigation applications use stabilizer platforms where sensors are placed on the platform and are isolated from rotational motions. The use of a stabilizer platform is still mandatory mainly for applications requiring the precision of navigation data such as on aviation [2].

Considering this context, our work introduces a *low-cost embedded system design and implementation for a two-axis camera platform control* used in UAVs. The proposed design cost is about USD 110 which is lower than the widely used Zenmuse-2d [3] (price of $\approx$ USD 500). The simulated and experimental implementations take into account the background of three different domains: mechanical, computing and electronics. The main goal is to have a gimbal able to stabilize a camera, with respect to UAV attitude, using *permanent magnetic synchronous motors* (PMSM) as actuators.

Our design also uses an *inertial measurement unit*, comprised of a 3-axis accelerometer and a 3-axis gyroscope, as sensors, a *proportional-integral-derivative* controller, and a 32-bit microcontroller unit (MCU).

The literature presents some works dealing with gimbals control in UAV. However, most of them cope with the motors modeled as a direct current (DC) motor. Our research takes into account a PMSM that has no brushes and physical commutator, considered more reliable (*i.e.*, life cycle of over 10,000 hours) and having better power consumption characteristics. In [4], the gimbal has only one axis, and the design of the motor is a conventional direct current, differently from the embedded systems proposed here that considers a two-axis platform. The work of [5] uses a PMSM, nevertheless its application is not for a UAV. The work basically comprehends motor modeling, iterative learning control, and adaptive sliding mode control. The authors of [6] used a brushless DC motor with non-sinusoidal switching technique. The work of [7] states that many of the gimbal control development is concerned to military applications, and it is also hard to find useful information on commercial uses. That work has used a DC motor model which is not the same model as used in our proposed design.

The remainder of this paper is organized as follows. Section II introduces the main concepts and fundamentals used throughout the research. Section III presents the proposed embedded system design and its implementation details including the software and hardware, motors, gimbal, control, and sensors. Section IV brings the modeling and the system implementation. Section V shows the results, and finally the Section VI summarizes the paper conclusions and some future work suggestions.

II. BACKGROUND

Our proposed embedded system design involves areas of mechanics, electronics, and computing. This section presents the main concepts used along with the research comprising these areas.

[1]Advanced Computing, Control & Embedded Systems Laboratory / FEM, University of Campinas – UNICAMP, Campinas, SP, 13083-860, Brazil {francoplf, dloubach, fioravanti}@fem.unicamp.br

978-1-5386-0956-9/17/$31.00

A. Gimbal Actuators

Gimbals are classified by the number of rotation axes which are usually equivalent to the number of actuators. The physical structure of these gimbals can be compared with robotic manipulators as they are made up of links and joints. When the links and joints are integrated and have some implemented control, the manipulators become robots [8].

The gimbal actuators are responsible for controlling both the position and the velocity of the camera that is installed on the end effector. Most of these actuators are three-phase brushless motors known as gimbal motors. Usually, this type of motor has more than one pair of poles per phase, and this number defines the relationship between the electric and mechanical angles [9]. The brushless motors include DC motors and PMSM, for instance. Brushless DC motors are typically characterized as motors having back electromotive force (back-EMF) as a trapezoidal waveform. PMSMs have sine wave back-EMF, and can be driven by sinusoidal waveform [10]. The three-phase sine waves inputs must be shifted to each other by 120 degrees. These sinusoidal waves are generated by high frequency, *i.e.* 32 kHz, pulse width modulation (PWM) as shown in Figure 1 (a). This PWM is responsible for rotating the motor as shown in Figure 1 (b). The sinusoidal switching technique has all three motor coils fed at the same time and torque is smoother than the torque with the square wave power supply [11].

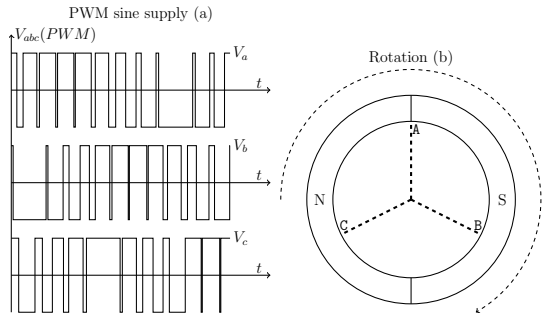

Fig. 1. Sine power supply

There are multiple ways to control the PMSM, including those using sine waves signals such as the present paper, square waves signals and field oriented control (FOC). The objective of the latter is to decouple the motor torque and the induction flow [11].

B. Real-Time Embedded Systems

According to [12], "embedded systems are computer systems with integration of hardware and software tightly coupled designed to perform a particular function". Those systems are strictly interconnected to their environment. This may lead to strong time constraints imposed by the need to interact with surrounding objects.

A basic definition of real-time system is a computing system that must respond within well defined time constraints. Therefore, the behavior of such systems depend equally on the correctness of their computational logic and on the time at which the result is given. Time is the main aspect of the system and it is strictly related to the environment where the system operates [12].

Figure 2 presents a possible organization of an embedded system which can include an electromechanical subsystem. The latter can be compared to a gimbal in this research context. The figure also shows actuators, power supply, sensors, analog to digital conversion (A/D), and digital to analog (D/A) conversion. The processor together with the memory are responsible for operating the electromechanical subsystem according to the human interface and the external environment, for example.

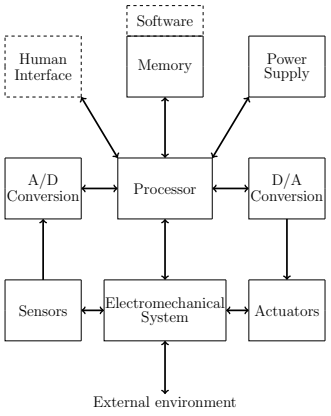

Fig. 2. Possible organization of an embedded system, adapted from [13]

III. PROPOSED EMBEDDED SYSTEM DESIGN

This section presents our low-cost embedded system design for controlling a two-axis gimbal. The proposed design considers the following major blocks: Software and hardware (SH); Drivers (DR); Motors (MT); Gimbal (GB); and Sensors (SE).

Figure 3 illustrates the design overview with blocks connections.

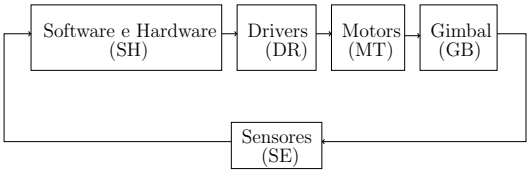

Fig. 3. Proposed embedded system design overview

The software and hardware (SH) block is based on the FRDM-KL25Z development kit. It has a 32-bit ARM Cortex-M0+ MCU that is widely used in research and development. The MCU is set to operate at its maximum core frequency, *i.e.,* 48 MHz.

The development environment of the SH block was the Kinetis Design Studio software (KDS), which is a GNU-based tool. It integrates the Processor Expert (PE) and also has open source software libraries such as the Kinetis Software Development Kit (KSDK) [14]. Sources

were built with the Cross-ARM GCC toolchain, version 2.1.1.201512141335.

The driver (DR) block applies an L6234 integrated circuit (IC). This is used as power supply for the three-phase PMSM. This IC is composed of 3 half-bridge drivers with maximum current of up to 5 A, and power supply voltages between 7 V and 52 V [15].

The motors (MT) block requires motors supporting low-speed movements (*i.e.*, $\approx$ 1 rpm) and they cannot have crimping problems. Furthermore, the motors must have enough torque to sustain and control the end effector. Therefore, the three-phase brushless motors that have sine wave back-EMF were chosen. These characteristics classify them as PMSM. Two motors were used in the MT block: one for the pitch control (BGM4108 130T), and the other for roll control (GBM2804 100T).

The mechanical structure for the gimbal (GB) block employed a commercial off-the-shelf platform. This platform was chosen because its mechanical construction is not this research focus. That mechanical structure allows for position adjustments on each rotation axis, and properly fits the motor fixing. The gimbal used was the DYS BLG3SN that has three degrees of freedom (DoF), although we are considering only two DoF.

Angular positions of each axis, *i.e.,* pitch and roll, connected to the rotors (θ_1 to BGM4108 130T and θ_2 to GBM2804 100T) can be obtained with an inertial sensor. The sensors (SE) block applied the MPU6050 IMU, which is responsible for measuring both the angular and linear accelerations of the end effector position considering a sampling rate of 200 Hz.

Instead of using directly angular position given by the IMU, a complementary filter was used to compute the end effector angular position. The work of [16] also used a solution with a complementary filter combining data from the gyroscope and accelerometer to improve the measurement confidence.

IV. SYSTEM IMPLEMENTATION

This section presents the kinematics and dynamics modeling along with the controller and embedded system implementations.

A. Kinematics Model

The mechanism of the two-axis gimbal can be represented as shown in Figure 4. The gimbal can be installed on the bottom of a UAV, and the rotations of the two gimbal motors must be limited to avoid any mechanical shock. The mechanism kinematics model assists in the identification of the gimbal workspace and the control of the end effector position. Therefore, we applied the Denavit-Hartenberg (DH) method. In this case, the reference frames are O_0, O_1 and O_2 as shown in Figure 4. The DH parameters are presented in Table I. It is important to note that the reference frame O_2 represents the last position of the end effector. We obtained the transformations between the references O_0 and O_2 given by T_0^2 according to Equation (1).

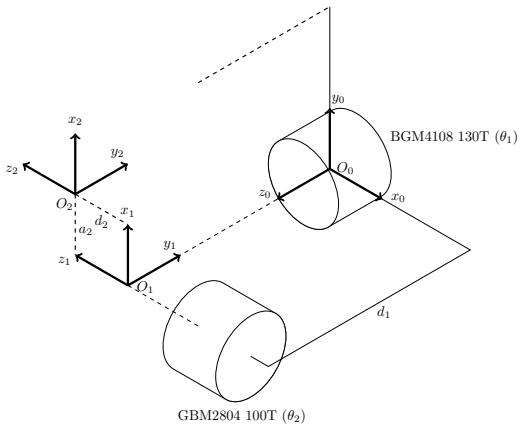

Fig. 4. Definition of the platform axes

TABLE I
PLATFORM DH PARAMETERS

Link	a_i	α_i	d_i	θ_i
1	0	$\frac{-\pi}{2}$	d_1	θ_1
2	a_2	0	d_2	θ_2

$$T_0^2 = \begin{bmatrix} C_{\theta_1}C_{\theta_2} & -C_{\theta_1}S_{\theta_2} & -S_{\theta_1} & a_2C_{\theta_2}C_{\theta_1} - d_2S_{\theta_1} \\ S_{\theta_1}C_{\theta_2} & -S_{\theta_1}S_{\theta_2} & C_{\theta_1} & a_2C_{\theta_2}S_{\theta_1} + d_2C_{\theta_1} \\ -S_{\theta_2} & -C_{\theta_2} & 0 & -a_2S_{\theta_2} + d_1 \\ 0 & 0 & 0 & 1 \end{bmatrix} \quad (1)$$

The workspace of the camera center (Fig. 5) is obtained by Equation (1). The angles θ_2 and θ_1 are in the range of $\frac{-\pi}{4} < \theta_{1,2} < \frac{\pi}{4}$; $d_1 = 70$ mm; $a_2 = 15$ mm; and $d_2 = 35$ mm.

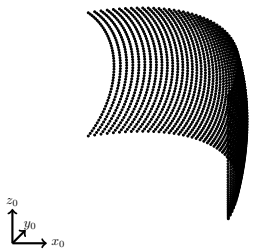

Fig. 5. Gimbal workspace

B. Dynamics Model

The gimbal control development depends mainly on the actuators control in all axes. The choice of actuators as PMSM complied with this type of system since such motors allow the control to perform at low speeds and high accelerations (*i.e.*, $30°/s^2$).

This system uses the sinusoidal switching technique and the controllers act on the phase (θ_e) of the three-phase sinusoidal supply (v_{as}, v_{bs}, v_{cs}) as illustrated in Figure 6. The sine wave is obtained by the application of a PWM signal at the input of the three-phase motor stator, which results in the rotor movement (θ_r). The main reason for this choice is the possibility of rotor control with slow rotation

and with no significant torque disturbances due to magnetic field interactions between the stator and the rotor.

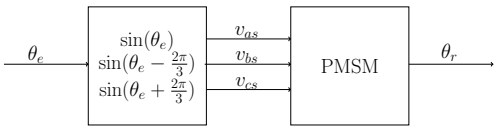

Fig. 6. Sine wave input power source

The PMSMs are modeled considering a rigid reference related to their rotors. This reference is known as the q-d Park's reference as illustrated in Figure 7, in which θ_r is the rotor angle. The input voltages v_{as}, v_{bs}, and v_{cs} (sinusoidal waves) of the three-phase stator can be obtained in the reference frame q-d of the rotor, according to a transformation matrix of the stator to rotor reference frame. Therefore the input voltages v_q and v_d are obtained in the q-d Park's reference according to Equation (2).

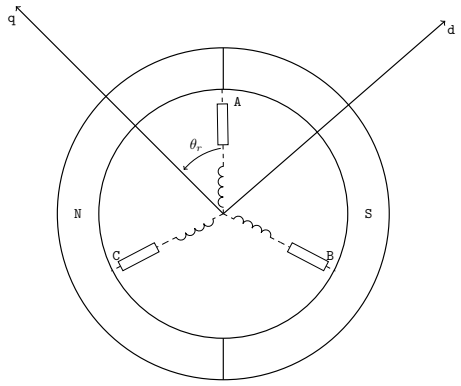

Fig. 7. PMSM and q-d Park's reference, adapted from [11]

$$\begin{bmatrix} v_q \\ v_d \\ v_0 \end{bmatrix} = \begin{bmatrix} -\sin(\theta_r - \theta_e) \\ \cos(\theta_r - \theta_e) \\ 0 \end{bmatrix} \tag{2}$$

In this reference, the PMSM electrical circuit is generally described by the Equations (3) and (4) [11].

$$v_q = R_s i_q + L_q \frac{di_q}{dt} + \omega_r L_d i_d + \omega_r \lambda_{af} \tag{3}$$

$$v_d = -\omega_r L_q i_q + R_s i_d + L_d \frac{di_d}{dt} \tag{4}$$

where R_s is the stator resistance; L_q and L_d are the stator inductance in q-d Park's reference; i_q and i_d are the currents in q-d Park's reference; ω_r is the rotor angular speed; and λ_{af} is the permanent magnet flux.

The electromagnetic torque of the motor can be expressed as:

$$T_e = \frac{3}{2}\frac{N_p}{2}[\lambda_{af} + (L_d - L_q)i_d]i_q \tag{5}$$

where N_p is the number of magnet poles.

The dynamic equation of the PMSM is represented as:

$$T_e - T_l = J\frac{d\omega_r}{dt} + B\omega_r \tag{6}$$

where T_l is the load torque; J is the total moment of inertia in the motor axis; and B is the coefficient of motor friction.

C. Controller

The controller used in this research was the PID. The controlled variable was the rotor angular position with respect to the gimbal position. The goal of the controller is to leave the end effector in the original position. The reference for this condition is $\theta_{ref} = 0$. The diagram shown in Figure 8 illustrates the control block diagram for the roll and the pitch controls.

The PID controller acts on the sine-PWM (SPWM) block. This is a discrete sine function whose outputs are duty-cycles with sine waves shifted 120 degrees from each other. The L6234 IC is responsible for the motor amplified PWM signal inputs. The MPU6050 sensor obtains the angular accelerations ($\ddot{\hat{\theta}}_{1,2}$) and linear accelerations ($\ddot{\hat{x}}_{1,2}$, $\ddot{\hat{y}}_{1,2}$, $\ddot{\hat{z}}_{1,2}$) values used to estimate the $\theta_{1,2}$ position, using the complementary filter previously mentioned.

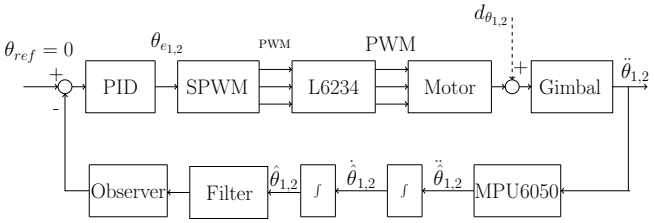

Fig. 8. Control block diagram

The PID controller indicates how to control the variables θ_{e_1} and θ_{e_2} which are the phases of the sinusoidal commutation. Thus, according to the disturbances, in this case the UAV attitude, d_{θ_1} at θ_1 and d_{θ_2} at θ_2 in the gimbal structure, the PID controller acts to leave the end effector stable at original position.

The motors control cycle has a frequency of 1 kHz. This is higher than the sensor reading cycle frequency that is 200 Hz. Therefore, positions observers ($\hat{\theta}_1$ and $\hat{\theta}_2$) are required to ensure that there is an estimated angular position at each motor control cycle. The observer was implemented as a third degree polynomial approximation considering the last four cycle computed values. A Kalman filter was not used due to the required computation time constraint of the control cycle (*i.e.,* 100 μs) and the available computational power.

The control block, illustrated in Figure 8, was simulated using Simulink R2015a. We used the PID Simulink block, where tuning is achieved firstly with the Ziegler and Nichols method [17]. The PID controller found according to that method was not satisfactory because the response to the disturbances caused oscillations to the gimbal. The primary controller goal is to handle motors responses that must be as fast as possible according to UAV attitude and without oscillations as long as they respect their saturation. Therefore, it was necessary to decrease the proportional gain (P) and increase the integral gain (I) to delay the response of the system. Furthermore, we found numerical difficulties considering the derivative term (D) because of sensor noises. The motors parameters (BGM4108 130T and GBM2804 100T) and the total moments of inertia in their axes were

experimentally obtained. These values are presented in Table II.

TABLE II
MOTORS PARAMETERS

Parameters	BGM4108 130T (θ_1)	GBM2804 100T (θ_2)
N_p	22	14
$R_s(\Omega)$	6.1	5
$L_q(H)$	2.44×10^{-3}	1.08×10^{-3}
$L_d(H)$	1.90×10^{-3}	0.823×10^{-3}
$\lambda_{af}(Wb)$	0.13	0.045
$J(Kg.m^2)$	0.022	8.9×10^{-4}
$B(N.m.s)$	7.7×10^{-4}	5.4×10^{-4}

D. Embedded System

The SH block implements the embedded software responsible for reading the sensors and controlling the motors, as presented in Figure 3.

The implemented method to integrate accelerations from the IMU was the trapezoidal rule. The angular position is also estimated using the arctangent approximation of linear accelerations.

V. RESULTS

Simulated and experimental results show that the developed embedded system was able to respond to a simulated UAV flight envelope, then reacting in real-time and minimizing those disturbances, as presented in this section.

First, a *simulated method* was performed. We tuned the PID controller based on the developed kinematics and dynamics modeling, taking into account the designed control block (Figure 8), introduced in Section IV. For this case, parameters P and I were obtained using the Ziegler and Nichols method and they were also tuned in order to reduce the system time using the Simulink and the Tune PID tool. The parameter D was not used because of the sensor noise. Therefore, the controllers used are PI controllers for both θ_1 and θ_2.

Next, an *experimental method* was carried out. We used the System Identification Toolbox (SIT) from Matlab to also tune PID parameters considering the same control block, but now considering the implemented embedded system instead of simulations. The SIT provides identification techniques such as maximum likelihood. In this case, we applied a known input in the physical system, *i.e.* gimbal, and recovered the results θ_1 and θ_2. With these input and output, SIT was able to return a second order linear model.

The values of the PI controllers for both methods are presented in the Table III.

TABLE III
PI CONTROLLERS

Motors	Simulated Method	Experimental Method
BGM4108 130T (θ_1)	P = 20; I = 74	P = 4.5; I = 1130
GBM2804 100T (θ_2)	P = 6; I = 24	P = 1.5; I = 600

The performance of the obtained PI controllers was analyzed based on the disturbances responses, pitch and roll movements, from the gimbal. Then, we measured both the disturbances and the responses on each axis, *i.e.* θ_1 and θ_2. Figures 9 and 10 show the responses to disturbances on the gimbal using the PI controller obtained from the simulated method.

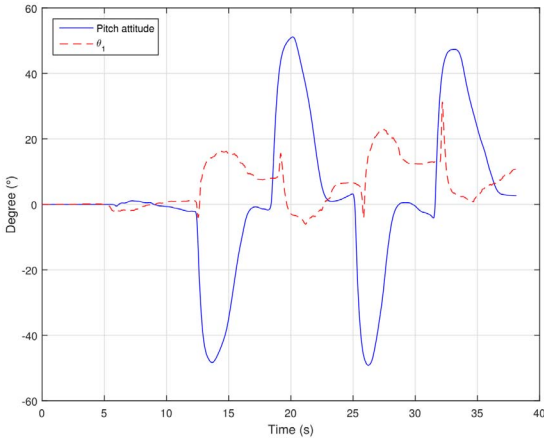

Fig. 9. θ_1 and pitch attitude

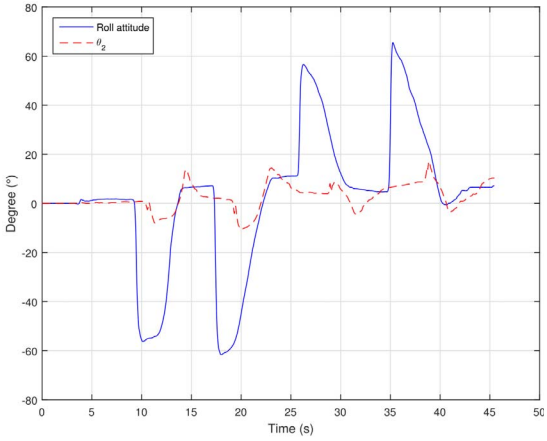

Fig. 10. θ_2 and roll attitude

Figures 11 and 12 show the responses considering the experimental method and disturbances from the end effector.

Both methods can stabilize the end effector angular position. However, the controller obtained by the simulated method has a shorter response time and smaller oscillations but greater final position errors. The controller obtained by the experimental method presents a higher response time, larger oscillations but lower errors about the reference position. The main difference between these two approaches is that, in the experimental method, the sensor is included in the obtained model. Therefore, the integral constant (I) increases mainly due to sensor noises.

The gimbal controller was implemented in a real-time embedded system. The Table IV shows the period and the execution time of the main functions from the control cycle.

According to the Table IV, f_1 execution time is about half of its period (42.9%), and f_2 takes 10% of its period.

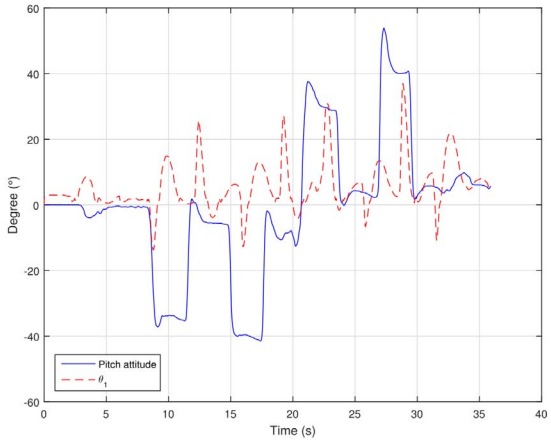

Fig. 11. θ_1 and pitch attitude

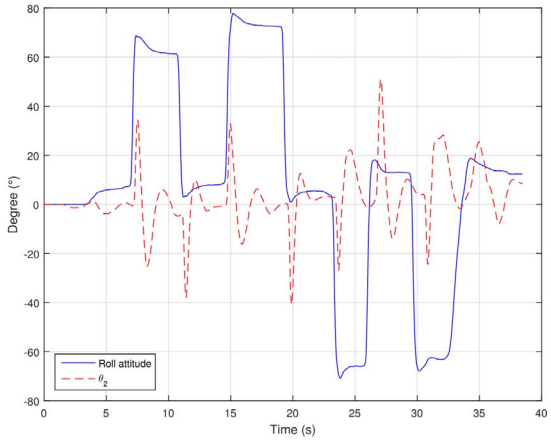

Fig. 12. θ_2 and roll attitude

TABLE IV
EXECUTION TIME OF THE FUNCTIONS IN THE CONTROL CYCLE

Function	Period (ms)	Exec. Time (ms)	%
(f_1) Reading, computation, filter and observer	5	2.145	42.9
(f_2) PI controller	1	0.100	10

Those two methods were considered satisfactory for low speed (*i.e.*, 1 rpm) and high accelerations (*i.e.*, $30°/s^2$). However, further research has to be carried out to improve the quality of the sensor data and thereby decrease the final position errors.

A short movie of the implemented system is available at *https://youtu.be/ciuk8FDK-qQ*.

VI. CONCLUSION

This paper introduced a low-cost embedded system design and implementation for a two-axis camera platform control used in UAVs. The design implemented a proportional-integral controller with two permanent magnetic synchronous motors (PMSM), an inertial measurement unit, and a 32-bit microcontroller unit.

The goal to have a gimbal able to stabilize a camera, with respect to UAV attitude, using PMSM was achieved although in the simulated method there were more significant final position errors. The PMSM are driven by a sinusoidal switching technique. Furthermore, these motors need an electronic controller to replace the commutator of the brushed direct current motor. Therefore, controlling a PMSM makes this research different from those controlling a brushed DC motor.

As future work, field oriented control (FOC) method could be applied to control the motor current and torque. This method allows transforming the non-linear model of the brushless motors into linear model also helping to minimize the ripple torque.

ACKNOWLEDGMENT

This research is supported by the Coordination for the Improvement of Higher Education Personnel (CAPES), scholarship 33003017, and the Regular Research Awards grant 2014/24855-8, São Paulo Research Foundation (FAPESP).

REFERENCES

[1] X. Kerasidou, M. Büscher, and M. Liegl, "Don't Drone? Negotiating Ethics of RPAS in Emergency Response," *Proceedings of the ISCRAM 2015 Conference*, 2015.

[2] D. Cuk and M. Ahmed, "Comparison of Different Computation Methods for Strapdown Inertial Navigation Systems," *Scientific-Technical Review*, 2005.

[3] "Zenmuse gimbal," https://www.dji.com/zenmuse-h3-2d, accessed: 2017-08-11.

[4] A. S. Kori, C. M. Ananda, and T. S. Chandar, "Robust control of single axis gimbal platform for micro air vehicles based on uncertainty and disturbance estimation," in *2016 7th International Conference on Mechanical and Aerospace Engineering (ICMAE)*, July 2016, pp. 480–486.

[5] Z. Lei, Z. Baichen, W. Dengyun, and L. Ming, "A low speed servo system of CMG gimbal based on adaptive sliding mode control and iterative learning compensation," in *2015 IEEE International Conference on Mechatronics and Automation (ICMA)*, Aug 2015, pp. 2249–2254.

[6] H. Yuewei, L. Ming, T. Limei, and Y. Jigang, "The research of different pulse width modulation strategies used in control moment gyro gimbal motor," in *The 27th Chinese Control and Decision Conference (2015 CCDC)*, May 2015, pp. 3393–3396.

[7] J. Johansson, "Modelling and control of an advanced camera gimbal," Master's thesis, Linköpings, Sweden, 2012.

[8] R. N. Jazar, *Theory of Applied Robotics*. Springer, 2006.

[9] P. Staszko, "Three-Phase BLDC Sensorless Motor Control Application," *Freescale Semiconductor,Design Reference Manual*, 2014.

[10] D. Hanselman, *Brushless Permanent Magnet Motor Design*. Magna Physics, 2003.

[11] R. Krishnan, *Permanent Magnet Synchronous and Brushless DC Motor Drives*. Taylor and Francis Group, LLC, 2010.

[12] Q. Li and C. Yao, *Real-Time Concepts for Embedded Systems*. CMP books, 2003.

[13] W. Stallings, *Computer Organization and Architecture: Design for Perfomance*. Pearson Education, 2013.

[14] Freescale, "Getting Started with Kinetis SDK (KSDK)," 2015, accessed: 2016-03-01. [Online]. Available: http://www.nxp.com/assets/documents/data/en/user-guides/KSDK13GSUG.pdf

[15] STMicroelectronics, "L6234 Three Phase Motor Drier," 2003, accessed: 2015-11-01. [Online]. Available: http://pdf1.alldatasheet.com/datasheet-pdf/view/164548/STMICROELECTRONICS/L6234.html

[16] V. M. D. M. Leite and A. G. S. Conceio, "Testbed prototype of an unmanned aerial vehicle design," in *2016 XIII Latin American Robotics Symposium and IV Brazilian Robotics Symposium (LARS/SBR)*, Oct 2016, pp. 340–345.

[17] J. G. Ziegler and N. B. Nichols, *Optimum settings for automatic controllers*. Transactions of the ASME, 1942.